IJNAOE
©SNAK, 2015

Int. J. Nav. Archit. Ocean Eng. (2015) 7:906~919
http://dx.doi.org/10.1515/ijnaoe-2015-0063
pISSN: 2092-6782, eISSN: 2092-6790

Experimental investigation of flow characteristics around four square-cylinder arrays at subcritical Reynolds numbers

Mingyue Liu, Longfei Xiao and Lijun Yang

State Key Laboratory of Ocean Engineering, Shanghai Jiao Tong University, Shanghai, China

Received 22 April 2015; Revised 23 June 2015; Accepted 5 July 2015

ABSTRACT: *The Deep Draft Semi-Submersible (DDS) concepts are known for their favourable vertical motion performance. However, the DDS may experience critical Vortex-Induced Motion (VIM) stemming from the fluctuating forces on the columns. In order to investigate the current-induced excitation forces of VIM, an experimental study of flow characteristics around four square-section cylinders in a square configuration is presented. A number of column spacing ratios and array attack angles were considered to investigate the parametric influences. The results comprise flow patterns, drag and lift forces, as well as Strouhal numbers. It is shown that both the drag and lift forces acting on the cylinders are slightly different between the various L/D values, and the fluctuating forces peak at L/D = 4.14. The lift force of downstream cylinders reaches its maximum at around α = 15°. Furthermore, the flow around circular-section-cylinder arrays is also discussed in comparison with that of square cylinders.*

KEY WORDS: Deep draft semi-submersible (DDS); Experimental study; Four square-section cylinders; Spacing ratio; Array attack angle.

NOMENCLATURE

A_p	Projected area normal to the flow direction	H	height of square cylinder
C_D	drag coefficient ($= F_x / (0.5 \times \rho U_\infty{}^2 A_p)$)	H / D	aspect ratio
$\overline{C}_D$	average drag coefficient for each cylinder	L	centre-to-centre cylinder spacing
C_L	lift coefficient ($= F_y / (0.5 \times \rho U_\infty{}^2 A_p)$)	L / D	spacing ratio
$\overline{C}_L$	average lift coefficient for each cylinder	Re	Reynolds number ($= U_\infty D / \nu$)
C_{Lrms}	root-mean-square value of lift coefficient	St	Strouhal number ($= f_v D / U_\infty$)
	for each cylinder	U_∞	free-stream velocity
D	width of square cylinder	α	attack angle
f_v	vortex-shedding frequency (*Hz*)	F_x	streamwise force component
F_y	cross-stream force component	ρ	air density
ν	kinetic viscosity of air		

Corresponding author: *Longfei Xiao*, e-mail: *xiaolf@sjtu.edu.cn*

INTRODUCTION

Recently the effect of the sea current environment on the dynamic behaviour of floating offshore structures has become an important design issue. Because of potentially resulting in significant fatigue damage of moorings and risers, more recent work has indicated Vortex-Induced Motion (VIM) in addition to semi-submersible platforms, particularly with the development of Deep Draft Semi-submersible (DDS) concepts. Waals et al. (2007) carried out model tests to discuss the dynamic behaviour and the associated complex flow patterns of DDS and Tension Leg Platforms (TLP) in current. Goncalves et al. (2012; 2013) performed a series of tests to check the effects of different factors on the VIM of a semi-submersible platform with four square columns, considering such as current incidence angles, hull appendages, surface waves, the external damping level and draft conditions.

As a multi-column floater, the deep draft semi-submersible experiences the VIM similarly to that of a group of bluff bodies exposed to a cross flow. Therefore, aiming to understand the hydrodynamic excitation forces and the fluid mechanism of the VIM behaviour, it is essential to study vortex shedding characteristics and the resulting induced forces from the cross flow around the column arrays. Liu and Chen (2002) reported an experimental study on the flow around two square cylinders in a tandem arrangement with the spacing between the centres of the cylinders varying from 1.5 to 9 times the width of the cylinder at the Reynolds number ranging from 2.0×10^3 to 1.6×10^4. The experimental investigation stated that the flow characteristics around two cylinders in tandem depended strongly not only on the spacing ratio, but also on the arrangement form. Hasebe et al. (2009) conducted an experimental study on two square cylinders in tandem arrangement, and pay more attention to the flow field between two cylinders. The surface pressure distributions and the velocity between two cylinders were measured. Agrawal et al. (2006) examined the low-Reynolds number flow around two square cylinders placed side-by-side using the lattice Boltzmann method. They demonstrated the existence of both synchronized and flip-flop eddy shedding regimes with square cylinders, in agreement with the well known results for circular cylinders. Kumar et al. (2008) presented a simulation of flow around a row of nine square cylinders placed normal to the oncoming flow with spacing to diameter ratios of 0.3 to 12 and undertaken by the lattice Boltzmann method. No significant interaction between the individual wakes was observed with a spacing greater than six times the diameter.

Studies of the more complex wake flow around four-square-cylinder arrangements are still rather scarce and have not been well documented in the literature. Some investigations of the flow patterns for four circular section cylinders have been carried out using both experimental and numerical techniques over the past few years. Lam and Lo (1992) and Lam et al. (2003a) conducted flow visualization studies in order to understand the effects of the spacing ratio on both the flow patterns and vortex shedding frequencies. Moreover, Lam and Fang (1995) and Lam et al. (2003b) measured the drag and lift coefficients and the pressure distributions on four cylinders in a square configuration with various spacing ratios and array attack angles. However, investigations of the spacing ratio and the array attack angle effects on the flow characteristics for four cylinders in an in-line rectangular configuration are far from completed, especially at high Reynolds numbers for turbulent flow conditions. The present work aims to experimentally study the flow dynamics around four cylinders (of both circular and square section) grouped in a square configuration at subcritical Reynolds numbers. Three spacing ratios and four angles of incidence were investigated. In this study, particular attention is paid to the flow field around square cylinders as they are being increasingly considered by designers.

EXPERIMENTAL SETUP

Test conditions

The experiments were carried out in a closed circuit low-speed wind tunnel with a test section (0.6 m × 0.8 m × 2.1 m, respectively, width × depth × length). The uniform flow into the test section had the maximum turbulence intensity 0.7% for the velocity ranged in the experiments. The four cylinder models, of 29 mm × 29 mm square cross-section and with a 20.5 aspect ratio, were always positioned vertically oriented on the longitudinal centre line of the working section. All models were constructed from stainless steel, and had machined sharp edges. Each cylinder was essentially a rigid inflexible element. The blockage ratio (per cylinder) in the test section was 4.8% for the present experiments. For the single cylinder tests, this blockage falls within the single cylinder blockage reported in West and Apelt (1982) and in Schewe (1983). According to Ota et al. (1994), the blockage correction applied to the drag coefficients was $\approx$ 10.5%, which was estimated using the method based on

the flow past a single bluff cylinder. For the multiple-cylinder case when regular shedding of vortices from the upstream was suppressed, the blockage correction should be less. The present data was collected mainly for comparing the differences in flow characteristics caused by variations of the cylinder spacing and attack angle, and thus none of the results presented were corrected for the possible effects of the blockage.

Fig. 1 schematically depicts the test system. A turntable, to which all of the cylinders were attached, with an angle scale indication was mounted stably on the solid floor base under the middle of the test section. In the floor of the tunnel test section, a hole was made slightly larger than the diameter of the support pillar, so that no tunnel mechanical vibrations could be transmitted to the test models. In order to determine the aerodynamic forces acting on the models, each individual cylinder together with a load cell installed on its lower end was mounted vertically on a circular turntable. For an aspect ratio (*H/D*) of less than 20, Stansby (1974) emphasized the necessity of using end plates with a suggested leading edge of at least 2.5*D* from the individual cylinder axis, in order to avoid the effects of the wall boundary layer and horseshoe vortexes. In the present configuration, a rectangular end plate (i.e. deflector) with streamlined leading and trailing edges, made of 12 *mm* thick five-layer plywood and being 1,400 *mm* in length and 500 *mm* in width was fitted. The influence of the deflector boundary layer itself had been estimated during the preliminary tests since it introduced an effect of its own to the flow around the cylinders. The present results indicated that the relative error in force measurements due to the deflector was just under 2.5%, thus the effect of the deflector was considered to be negligible in the following study.

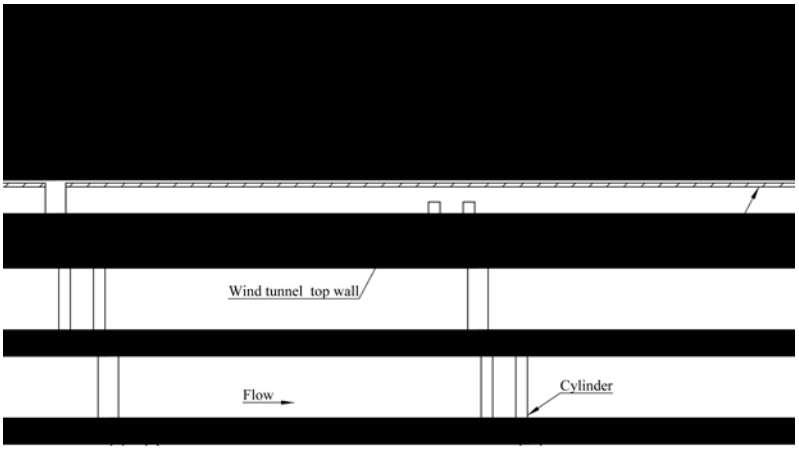

Fig. 1 A schematic of the cylinders assembly in the wind tunnel.

Experimental arrangement

The four cylinders were arranged in a square configuration as viewed from above (i.e. in the negative z direction), see Fig. 2. The uniform free-stream velocity is in the positive x direction, which is also the positive drag direction, while the positive lateral lift is defined as being in the positive y direction. The attack angle α was measured with respect to the line joining the centres of cylinders 3 and 4. The attack angle α was referred to as the array angle when the cylinders were considered as an array group and varied from 0° to 45°, increasing in 15° increments.

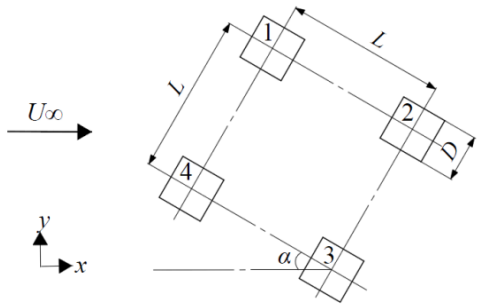

Fig. 2 The general configuration of the square cylinders model.

There were several holes arranged at different distances on the circular turntable, corresponding to different spacing ratio values (*L/D*) of the cylinder array arrangements. Considering the size of test instruments and the blockage ratios, the maximum allowable *L* value was 150 *mm*, while the minimum one was 100 *mm*. Therefore, three different *L/D* values were taken as 3.45, 4.14 and 5.17. The wind tunnel sidewall effects were considered to be insignificant, even for the 45° rotated maximum square configuration of *L/D* = 5.17. In the configurations examined, the smallest distance between the centre of any cylinder and the sidewall of the wind tunnel was approximately 6.7*D*. Some researches about vortex shedding frequency and associated flow patterns have indicated that 5*D* is adequate to minimize to an acceptable level of the proximity effects. Various reported numerical studies with a similar range of transverse distances to the tunnel side wall can confirm this estimation. In the numerical simulations of Li et al. (1992) and So et al. (2001), the transverse distance to the wall was 5*D*, whilst 7*D* was set in the work of Tutar and Holdø (2001).

Force measurements

A piezo-electric load cell can give the integral force directly with high response, resolution and stiffness. Therefore, this direct method to measure the spanwise averaged mean and fluctuating forces acting on a single cylinder had been used by Savkar (1981), Lam et al. (2003b) and Alam and Zhou (2007). In this study, aerodynamic force signals acting on each cylinder were recorded by the three-component quartz piezoelectric load cell (Kyowa LSM-B-500NSA1-P) at the base of each cylinder, as noted earlier. Savkar (1981) suggested that the natural response frequency of the load cell is required to be at least four times that of the dominant force frequency, in order to function with reasonable accuracy. In this work, the natural frequencies of the load cell in the x and y directions were both 2.2 *kHz*, while the measured frequency of the fluctuating drag and lift forces ranged from 20 *Hz* to 300 *Hz*. Consequently, it was considered that the fluctuating forces could be measured without introducing a potential resonance problem. As shown in Fig. 1, each load cell mounted on the bottom end of each cylinder was bolted tightly on the stainless steel block, which led to the load cells themselves being also in the flow field. However, the present study verified that there were nearly no apparent effects on the force measurements, which could be ascribed to the proper size of the deflector and load cells own good performance. A static calibration of the load cells in the drag and lift directions was undertaken by using a simple system of dead weights. It was recognised that the same concentrated load acting on the cylinder could produce a slight decrease of the voltage output as the moment arm being increased. Thus three different weights were used to induce the output of the load cell to have a constant voltage at the origin, and this was done by adjusting the scale coefficients of the charge amplifiers linearly, which was the approach employed by Lam et al. (2003b).

Flow visualization

The complex patterns of flow field were recorded and visualized using the technique of the high-speed camera (PCO.1200 *s/hs*) and the supplement of a smoke generator in the wind tunnel. The resolution of the camera is 1280×1024 *pixels* and the exposure time can be varied from 1 to 20 *ms*. Hence the recording speed is fast enough to provide a single frame/multi-exposed image. A copper tube with an array of tiny outlet holes along its length, was used to continuously emit a stream of smoke. The flow visualization was performed at a *Re* value of around 4.06×10^3. Unfortunately, insufficient quality of the results were available from this part of the experimental study, which may be due to the lack of both a proper laser source and a method of the injection of fluorescent particles in the wind tunnel tests. However, the video of vortex flow patterns can be beneficial to understand the force characteristics.

RESULTS AND DISCUSSION

The experiments were carried out at different free stream velocities, which were selected as 2.1, 4.9, 9.4, 16.6, 23.7, and 30.1 *m/s* for all cases, corresponding to values of *Re* = 4.06×10^3, 9.55×10^3, 1.81×10^4, 3.22×10^4, 4.58×10^4, and 5.82×10^4, respectively. Because the mean force measurements listed in Table 1 do not show significant changes for the given *Re* numbers, only the results of load cell measurements at 23.7 *m/s*, i.e., at *Re* of 4.58×10^4, are presented in this paper. Owing to the better flow visualization measurements at *Re* of 4.06×10^3, however, the flow patterns will be shown based on this different *Re* number.

Table 1 Mean drag coefficients of a single square cylinder and the four-cylinder case at α = 0° with different *Re*.

Re	Mean drag coefficient $\overline{C}_D$		
	A single square cylinder	Four-cylinder arrays at L/D = 3.45	
		Cylinder 1	Cylinder 2
4.06×10^3	2.180	1.764	0.836
9.55×10^3	2.107	1.633	0.703
1.81×10^4	2.201	1.602	0.697
3.22×10^4	2.090	1.571	0.807
4.58×10^4	2.084	1.556	0.816
5.82×10^4	2.020	1.545	0.822

Validation of the test technique on a square cylinder

Aiming to validate the reliability of the measuring system, the aerodynamic characteristics of a single square cylinder at a zero angle of incidence to the flow were measured and compared with published results, see Table 2. Alam et al. (2011) noted that values of $\overline{C}_D$, C_{Lrms} and St are all dependent on the experimental conditions such as the blockage ratio, aspect ratio, end effects and turbulent intensity. Therefore, there are slight differences among these data.

Table 2 Experimental comparison of aerodynamic characteristics data for a single square cylinder.

Research	$Re\times10^{-4}$	Tunnel blockage Ratio (%)	Aspect ratio	Turbulent intensity	Force measurement technique	$\overline{C}_D$	C_{Lrms}	St
Nakaguchi et al. (1968)	2~6	-	-	Smooth	Pressure distribution	2.1	-	0.13
Bearman and Trueman (1972)	6.8	-	-	Smooth	Pressure distribution	2.19	-	0.13
Ootsuki et al. (1980)	6.5~7	-	-	0.2%	Pressure distribution	2.08	0.82	0.12
Lesage and Gartshore (1987)	3.3	4.1	18	-	Pressure distribution	2.04	1.33	0.13
Knisely (1990)	2.2	5	12	0.5%	Load cell	2.05	1.0	0.13
Norberg (1993)	1.3	4.7	51	Smooth	Pressure distribution	2.16	-	0.132
Lyn et al. (1995)	2.14	-	-	-	LDV	2.1	-	0.132
Tamura and Miyagi (1999)	3	5	6	0.5%	Load cell	2.1	1.05	0.128
Noda and Nakayama (2003)	6.89	4	10	0.2%	Pressure distribution	2.164	1.18	0.131
Alam et al. (2011)	4.7	3.5	7	0.5%	Load cell	2.15	1.18	0.128
Yen and Liu (2011)	2.1	4	25	0.4%	Pressure distribution	2.06	-	0.132
Present measurement	4.58	4.8	20.5	0.7%	Load cell	2.084	1.1	0.135

The Reynolds number in the referred studies varied over the subcritical *Re* range and with the corresponding drag coefficients falling within the range 2.04 to 2.19. The maximum deviation among the drag coefficients published in the literature with that from the present work is less than 4.9%. The agreement can hence be considered satisfactory. Saha et al. (2000) commented that the drag coefficient is insensitive to the Reynolds number in the subcritical flow regime. This agrees well with the generally recognised observation that the dimensionless flow characteristics of the square cylinder are independent of the Reynolds number, primarily due to the points of flow separation always appearing to be at the sharp corners. There is relatively large scattering in the root mean square value of the lift coefficient (C_{Lrms}), ranging from a low value of 0.82 to a high value of 1.33. Different techniques have been used to measure the fluctuating lift force, which is largest when measured from the pressure distribution around an elemental section. Furthermore, C_{Lrms} is highly sensitive to the measurement length of the cylinder (West and Apelt, 1997), and decreases with an increasing measurement length. The Strouhal number for a square cylinder wake at a zero incident angle has been found to lie between 0.122 and 0.143 for a Reynolds number range of 1×10^4 to 1.2×10^5. The deviation between the present St number, 0.135, and others referred here is quite small. The near-constancy of the Strouhal number is again related to the fixed position of the flow separation points. The above comparisons provide a validation for present measurements.

The forces and the associated St of a single square cylinder at various angles of incidence were also measured in the present tests. The time-averaged drag coefficients and the Strouhal numbers for a square cylinder as a function of the incident angle are shown in Fig. 3. The variations of the drag coefficient and the Strouhal number with the angle are both not monotonic. The drag coefficient shows a reduction with respect to the angle from 0° to 15°, while the Strouhal number increases sharply. Smaller changes are seen for other values of the incident angle.

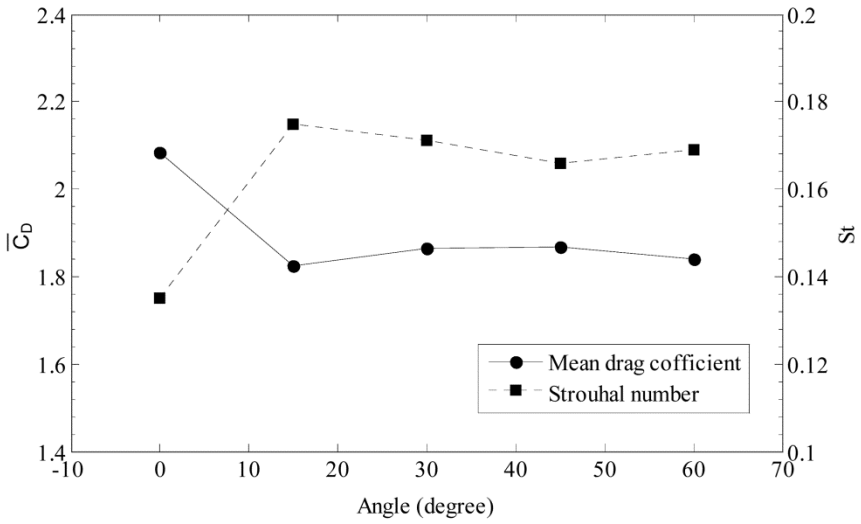

Fig. 3 The mean drag coefficients and Strouhal numbers for a single square cylinder as a function of the flow incident angle.

In order to explain the trends of the drag coefficient and the Strouhal number with respect to the incident angle, flow visualization studies were conducted in the wind tunnel at a *Re* of around 4.06×10^3. This work was undertaken, as described earlier, by using the high-speed camera and the smoke generator. The recorded images are presented in Fig. 4. It can be seen that the flow separation points for $\alpha = 0°$ are at the cylinder corners exposed to the approaching flow. At other higher angles, however, the flow separation is delayed up to the cylinder corners on the downstream side. There is a greater pressure recovery for all angles of inclination larger than zero. This effect is contrasted against the increase in the projected transverse dimension blocking the flow. The second factor is considered to be more important than the first one, which can be inferred from Fig. 3. Thus the drag coefficient based on the projected area A_p decreases with the incident angle increasing. The trend clearly reverses after 45° as a result of the symmetry.

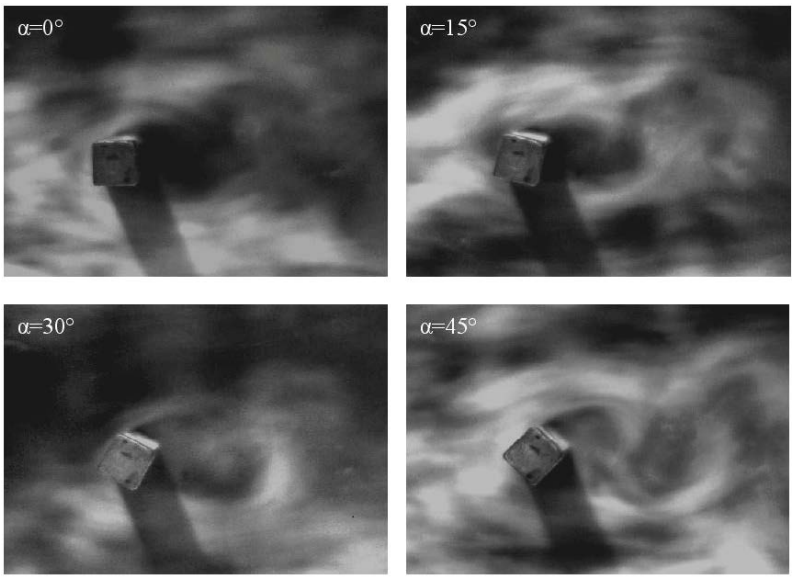

Fig. 4 Smoke aided visualization of the flow around a single square cylinder at various incident angles.

The variation of the Strouhal number with the angle can also be interpreted from Fig. 4. The trend of the Strouhal number can also be explained on the same basis as that of the variation of the mean drag coefficient. The modest decrease of the mean drag coefficient to a minimum at an angle of 15° is thought to be associated with a minimum wake width, corresponding to a minimum longitudinal vortex spacing, if a constant ratio of vortex spacing to wake width is assumed. This would result in an increase of the vortex-shedding frequency, and hence in an increase of the Strouhal number.

In-line square array

At α = 0°, the four-cylinder array is an in-line square configuration. Fig. 5 shows a typical picture of the flow pattern, which was carried out in the wind tunnel for L/D = 3.45 at Re = 4.06×10^3. From the flow visualization record, it can be observed that the interference between two cylinders in tandem would be much more severe than that between their side-by-side counterparts at and above the illustrated L/D ratio. Furthermore, it was seem that below a critical spacing, the downstream cylinders were always in the shadow of the upstream ones and vortex shedding were only observed for the downstream cylinders.

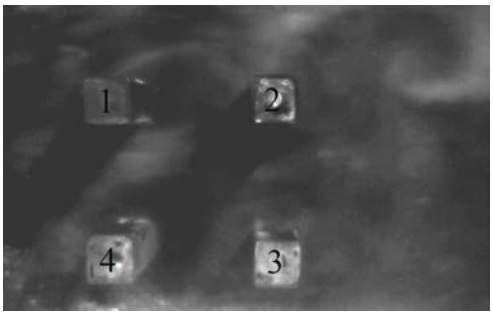

Fig. 5 A typical flow pattern of the four square cylinder arrays at α = 0° for L/D = 3.45.

At certain relatively large L/D ratios, the in-line square arrangement can be regarded as being essentially two parallel rows of two cylinders in tandem. Because of the complex flow interference between the upstream and downstream cylinders being the pivotal mechanism, reviewing the interactions of tandem square cylinders would be helpful to understand the more complex flow of the in-line square arrangement. Sakamoto et al. (1987) have experimentally investigated the flow field

around two tandem square cylinders. Their results showed that regular shedding of vortices from the upstream cylinder was suppressed when $L/D < 4$, and periodic vortex shedding initiates for $L/D = 4$. As investigated and generalized by Hasebe et al. (2009), the flow field between two cylinders showed two different patterns at $L/D = 4$, and these flow patterns vary periodically between two square cylinders in tandem arrangement. One is a diagonal flow which intersects between two cylinders. The other is a high curvature flow which forms the upward (downward) flow behind the upstream cylinder and the downward (upward) flow in the front of the downstream cylinder. According to Luo et al. (2003), for the stability issues when flow moved uniformly around two identical square cylinders, the magnitude of asymptotic C_D for $L/D \leq 4$ was smaller than that for $L/D > 4$. With $L/D \leq 4$, the associated flow structure is the reattached flow, and the downstream cylinder is subjected to a negative drag. In the range of $L/D > 4$, both cylinders shed vortices and the flow structure is called a co-shedding flow.

The Strouhal number (*St*) was obtained from a spectral analysis of the fluctuating lift force using a Power Spectral Density (PSD) plot. At $\alpha = 0°$, cylinders 1 and 2 and cylinders 4 and 3 are symmetrical, i.e., two parallel rows form a mirror image of each other. Two typical PSD plots for the fluctuating lift forces of cylinders 1 and 2 at $L/D = 3.45$ are shown in Fig. 6. For other *L/D* ratios, similar PSD plots were obtained, which are not given in this paper to avoid repetition. The electromagnetic interference component in the signal was fairly strong, which has thus been filtered out in present analysis. However, vortex shedding frequencies at these *L/D* ratios were also detected. All St were inferred from these PSD plots.

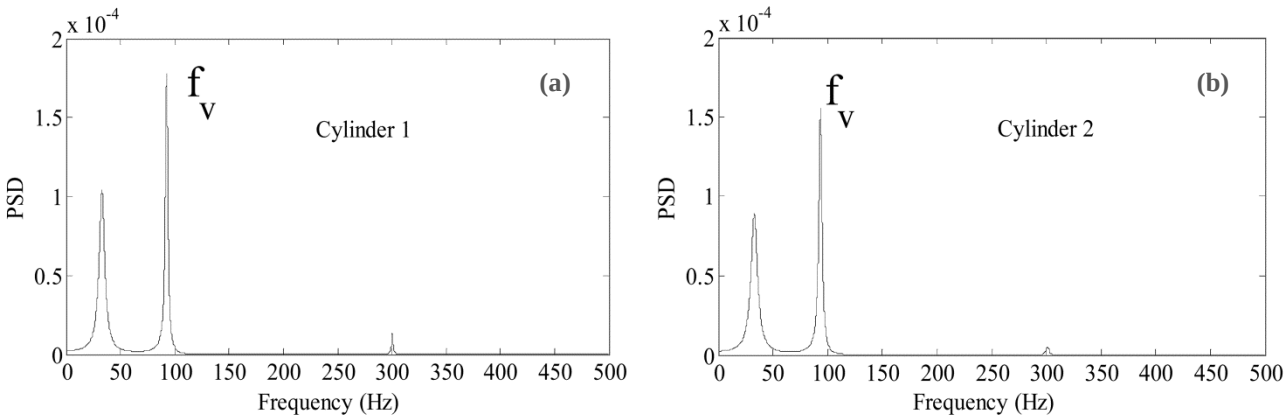

Fig. 6 The power spectral density (PSD) of the fluctuating lift force vs. frequency at $\alpha = 0°$ for $L/D = 3.45$.

Fig. 7 presents the variation of the force coefficients and the St number vs. *L/D* at $\alpha = 0°$. As for the mean forces, the mean drag coefficient ($\overline{C}_D$) of the upstream cylinders is found to be more than double that of downstream cylinders. Furthermore, all of the values are nearly stable at these *L/D* ratios and are smaller than that of a single cylinder case. In the four-cylinder configuration, the flow interference between all cylinders is more complex. The wakes of upstream cylinders are always affected not only by the downstream cylinder, but also by the side partners. This effect may disappear at sufficiently large spacing ratios. However, the range of the *L/D* ratios in the present tests is not large enough to show the trend that the $\overline{C}_D$ of the upstream cylinder tends to be close to that of a single cylinder as the *L/D* increases. The mean lift coefficient ($\overline{C}_L$) for cylinder 1 is negative at $L/D = 3.45$. The negative behaviour manifests that the up and down cylinders are effectively repelling each other. These results for the upstream cylinders further show a gradual increase to the same level of that for a single cylinder with *L/D* increases, owing to more and more insignificant side-by-side effect. It is interesting to note that the fluctuating lift force coefficients (C_{Lrms}) of both cylinders increase swiftly to their maximum values at $L/D = 4.14$, and then reduce sharply. With *L/D* increasing from 3.45 to 4.14, the location might correspond to the transition of flow pattern from a shear layer attachment to a vortex shedding flow. On the other hand, the fluctuating force coefficients at $L/D = 5.17$ are closer to that of a single square cylinder, which means that the interference between each cylinder becomes to be relatively weak. The Strouhal numbers, however, are not very distinct with changes in spacing ratios for both cylinders, which may be due to the flow separation point fixed at the sharp edge corners.

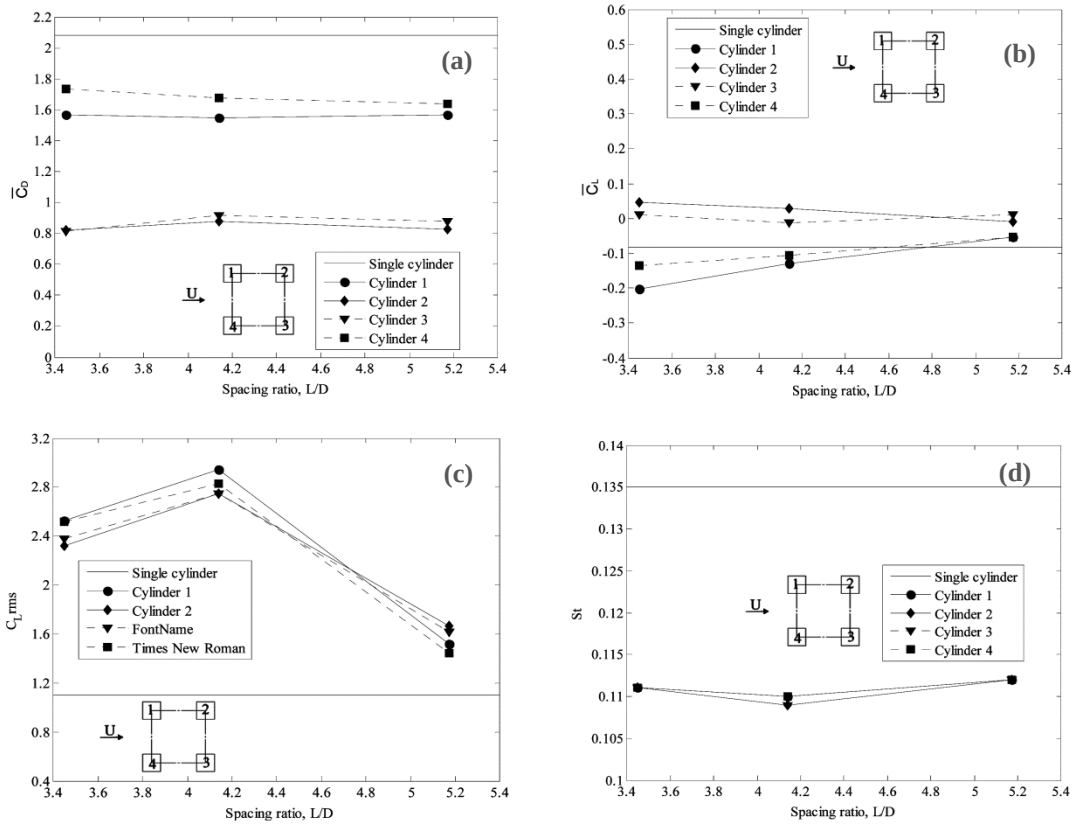

Fig. 7 The variation of force coefficients and St for a single cylinder and four-cylinder arrays at α = 0°: (a) mean drag force coefficient; (b) mean lift force coefficient; (c) fluctuating lift force coefficient; (d) Strouhal number.

Staggered angles

Fig. 8 shows the flow visualization results at α = 15° and 30° for Re = 4.06×10^3 as obtained in the wind tunnel tests. Cylinders 2 and 3 rotate to a low position compared with cylinders 1 and 4 at α = 15°. Cylinders 2 and 3 were partially immersed in the wake of the upstream cylinders, thus the flow phenomenon of shear layer reattachment can be seen. The downstream cylinders would experience an oscillating flow initiated by the upstream cylinders, consequently higher levels of fluctuating lift forces were anticipated. With α increasing to 30°, cylinder 2 becomes located downstream and between the trailing flows of cylinders 1 and 4, and thus a bypassing vortex could form near to cylinder 2. Its influence on the fluctuating lift forces becomes severe only at a relatively small L/D ratios. At the same time, cylinder 3 becomes relatively below cylinders 1 and 4, and experiences correspondingly less fluctuations in lift forces.

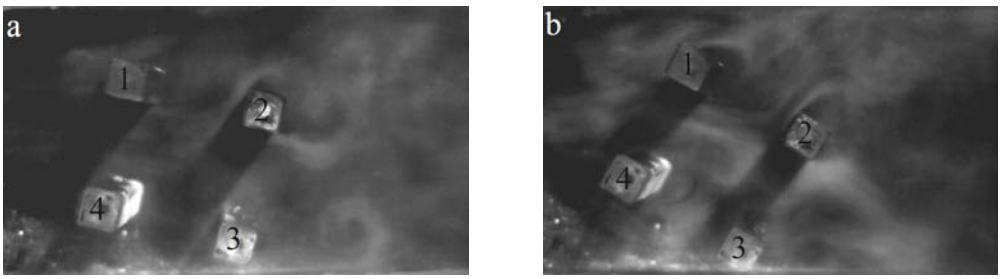

Fig. 8 Typical flow patterns at L/D = 3.45 in the wind tunnel: (a) α = 15°; (b) α = 30°.

The individual behaviour of the force coefficients and St for α = 15° and 30° are presented in Figs. 9 and 10, respectively. In these two flow directions, cylinder 2 was always immerged in the wake of the upstream cylinders, and this leads to the drag forces acting on cylinder 2 to be the smallest.

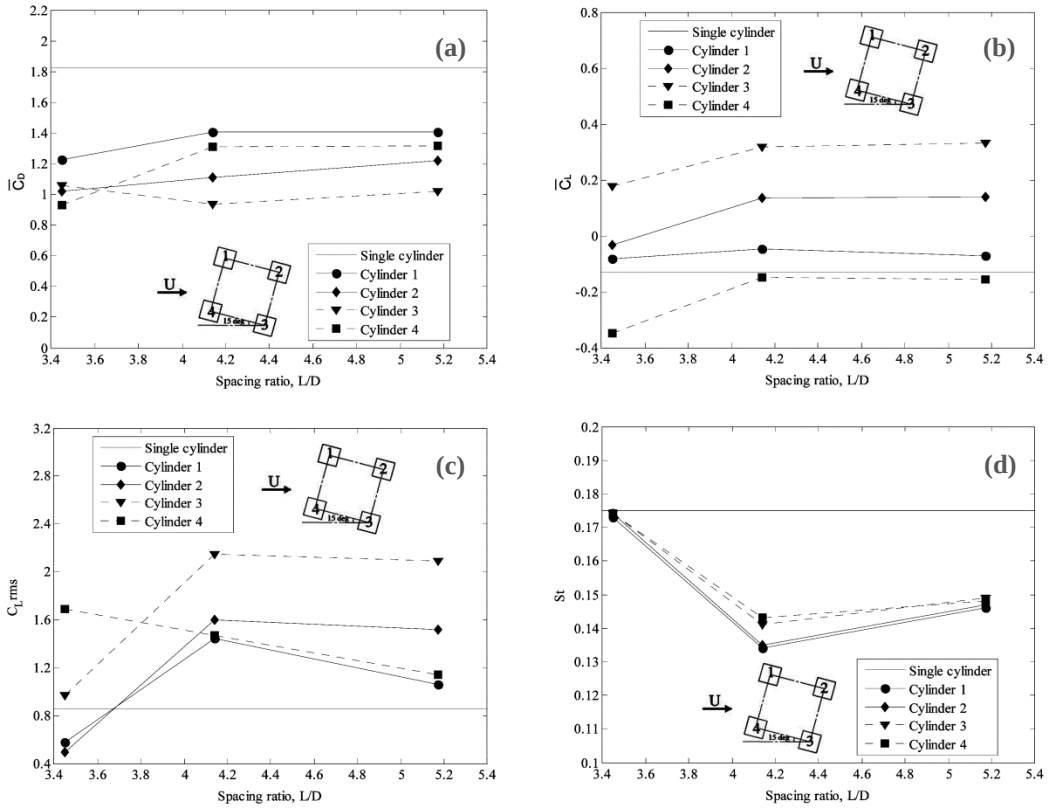

Fig. 9 The variation of force coefficients and St for a single cylinder and four-cylinder arrays at α = 15°:
(a) mean drag force coefficient; (b) mean lift force coefficient; (c) fluctuating lift force coefficient; (d) strouhal number.

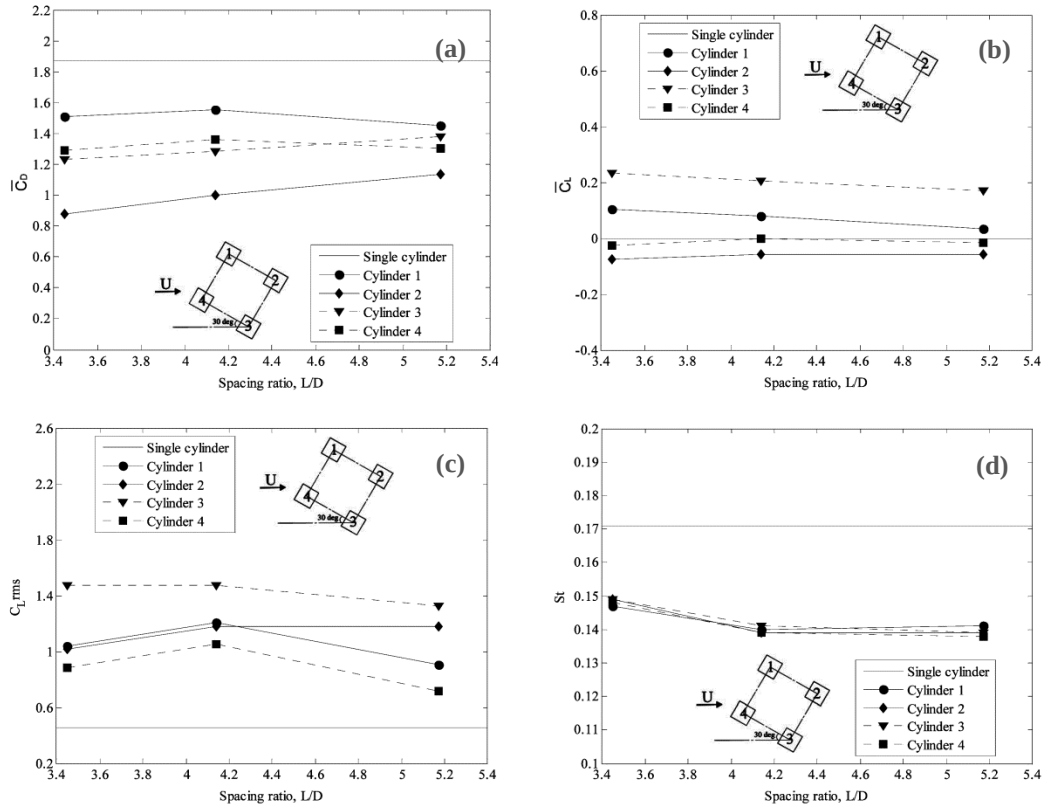

Fig. 10 The variation of force coefficients and St for a single cylinder and four-cylinder arrays at α = 30°:
(a) mean drag force coefficient; (b) mean lift force coefficient; (c) fluctuating lift force coefficient; (d) strouhal number.

At α = 15°, the variation of the measured lift force can be explained as follows. The first and most effected, cylinder 3 is partially immersed in the almost stationary wake of cylinder 4, which has a lower pressure. There is one further point to be noted that the gap between cylinders 2 and 3 is large enough not to exert a significant downward lift force on cylinder 3. Cylinder 2 is also immersed in the wake of cylinder 1. However, the stagnation pressure of the wake of cylinder 4 in the gap flow region just under cylinder 2 is low. Therefore, the $\overline{C}_L$ of cylinder 2 is not as large as that of cylinder 3. At α = 30°, the shedding vortices from cylinder 4 always impinge on the surface of cylinder 2 and entrain into the gap between cylinders 2 and 3, corresponding to lower pressure region under cylinder 2. This leads to a negative lift force on cylinder 2. Due to the low-pressure region between cylinders 2 and 3, the lift force acting on cylinder 3 is always positive and increases to high value at small *L/D* ratios. Furthermore, at α = 15°, a sharp drop is noticed for C_{Lrms} of cylinders 2 and 3 with *L/D* decreasing to 3.45. The smaller the *L/D*, the weaker becomes the oscillation of the shear layer of the upstream cylinders. The variation of the fluctuating forces is milder at α = 30°.

Rotated square arrangement

The array gives a rotated square configuration at α = 45°. Fig. 11 presents the measured forces and St of all cylinders. The arrangement is symmetrical, thus the force characteristics of cylinder 3 consistently match with those of cylinder 1. Cylinder 2 is located directly downstream of cylinder 4, thus cylinder 2 would be impinged continuously by the vortices being shed from cylinder 4. The C_{Lrms} of cylinder 2 thus becomes relatively large compared with that for a single square cylinder. Due to cylinders 1 and 3 being effectively located upstream and on both sides of cylinder 2, this would lead to the flow around cylinder 2 being the most seriously disturbed. Hence, it is impossible for cylinder 2 to be completely shielded by cylinder 4. As for $\overline{C}_L$, at this range of *L/D* ratios, the $\overline{C}_L$ for every cylinder remains at a relatively small value. Located directly downstream of cylinder 4, the drag force on cylinder 2 is smaller than that of cylinders 1 and 4.

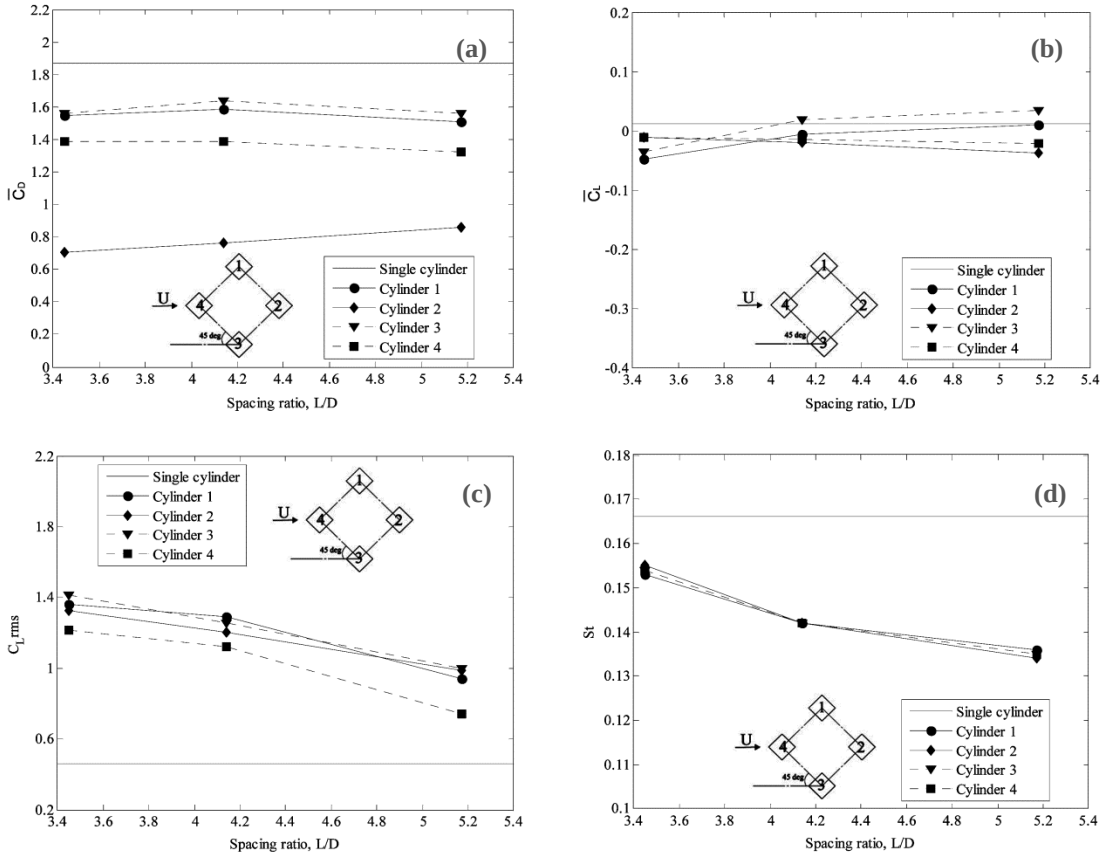

Fig. 11 The variation of force coefficients and St for a single cylinder and four-cylinder arrays at α = 45°: (a) mean drag force coefficient; (b) mean lift force coefficient; (c) fluctuating lift force coefficient; (d) strouhal number.

Effect of the cylinder's cross-section shape

The flow around four circular section cylinders arranged in a square configuration was also examined in this experimental work. The results for both the square and the circular section cylinder arrays at L/D = 4.14 are presented in Fig. 12. The two forms of section arrangements have a similar trend in their drag coefficients with flow angle α. At the in-line configuration (α = 0°), the $\overline{C}_D$ values of upstream cylinders are more than double those of downstream cylinders. Cylinder 2 was always located in the wake of the other upstream cylinders at all flow angles, and the $\overline{C}_D$ of cylinder 2 reaches its maximum value for both sections at α = 15°. The same behaviour between the square and circular cylinder arrays can also be noticed in the lift coefficient. The largest $\overline{C}_L$ for cylinder 2 is found at α = 15°, and then decreases sharply to a negative value at α = 30°, whereas the $\overline{C}_L$ for cylinder 3 is always positive. At α = 45°, the lift force coefficient for every cylinder stays at a relatively small value. This can be explained by the fact that the flow past each cylinder is symmetrical at a rotated square configuration and that the interference is very weak at a relatively large L/D ratio. The variations of the fluctuating lift force for the four square cylinders at different attack angles range widely and drop swiftly from very large values at α = 0° to relatively low values as α increases. On the other hand, the C_{Lrms} of four circular cylinders change slightly with different angles, and the C_{Lrms} of downstream cylinders are always larger than those of upstream cylinders. As for square cylinder arrangement, it is observed that the relationship of fluctuating lift forces between each cylinder is relatively irregular. It is to be noticed that circular cylinders act like a single cylinder at large attack angles, while the square cylinders tend to interact each other.

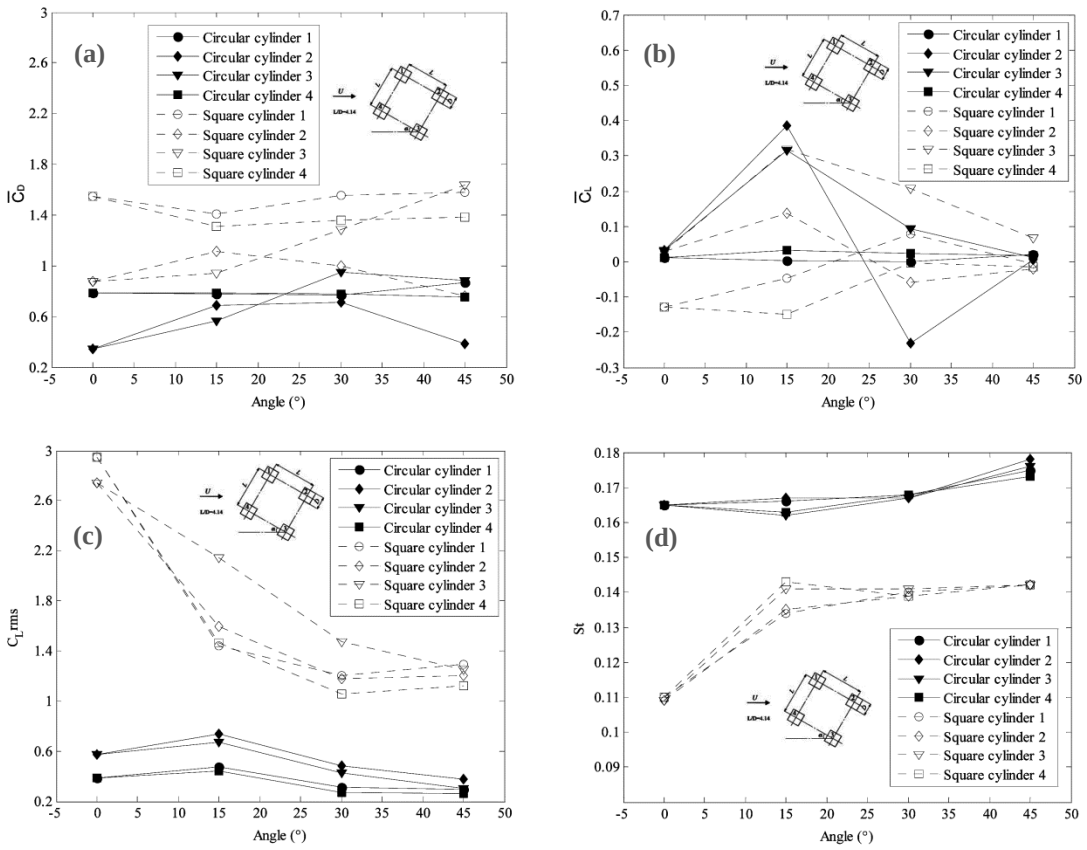

Fig. 12 The variation of force coefficients and St for four square cylinders and four circular cylinders at L/D = 4.14: (a) mean drag force coefficient; (b) mean lift force coefficient; (c) fluctuating lift force coefficient; (d) strouhal number.

CONCLUSIONS

A range of experiments on the flow characteristics around an array of four square-section cylinders in a square configuration have been carried out in a wind tunnel. The results at Re =4.58×10^4 are presented in this paper, covering three different spacing ratios (L/D = 3.45, 4.14 and 5.17), and four different array attack angles (α) ranging from 0° to 45° at intervals of 15°.

The results show that both the drag and the lift forces acting on the individual cylinders are slightly different among the tested different *L/D* values. The fluctuating forces, being the results of the development of trailing vortices, do not remain stable and peak at *L/D* = 4.14.

At α = 0°, the drag force on the downstream cylinders is half of that on the upstream cylinders. The downstream cylinder reaches its maximum lift force and experiences lower drag force at α = 15°. At the rotated configuration, α = 45°, the force characteristics of each cylinder are similar, which means that the interference between each other is relatively slight.

Being located in the complex wake of the upstream cylinders, the downstream cylinders are usually subjected to smaller mean drag forces than the upstream ones, whereas they would experience higher fluctuating forces. These were also realized by the results from the four circular cylinders tests. However, the flow around square cylinders is more complex and the fluctuating forces are relatively irregular. More effective visualization studies need to be performed, in order to explain and understand the force characteristics better.

ACKNOWLEDGEMENT

The authors would like to thank the support of the National Natural Science Foundation of China (Grant No.51279104) and a research project on high-technology ships supported by the Ministry of Industry and Information Technology of China.

REFERENCES

Agrawal, A., Djenidi, L. and Antonia, R.A., 2006. Investigation of flow around a pair of side-by-side square cylinders using the lattice Boltzmann method. *Computers & Fluids*, 35(10), pp.1093-1107.

Alam, M.D. and Zhou, Y., 2007. Turbulent wake of an inclined cylinder with water running. *Journal of Fluid Mechanics*, 589, pp.261-303.

Alam, M., Zhou, Y. and Wang, X.W., 2011. The wake of two side-by-side square cylinders. *Journal of Fluid Mechanics*, 669, pp.432-471.

Bearman, P. W. and Trueman, D. M., 1972. An investigation of the flow around rectangular cylinders. *Aeronaut. Q.* XXIII (Pt 3), pp.229-237.

Goncalves, R.T., Rosetti, G.F., Fujarra, A.L.C. and Oliveira, A.C., 2012. Experimental study on vortex-induced motions of a semi-submersible platform with four square columns, Part I: Effects of current incidence angle and hull appendages. *Ocean Engineering*, 54, pp.150-169.

Goncalves, R.T., Rosetti, G.F., Fujarra, A.L.C. and Oliveira, A.C., 2013. Experimental study on vortex-induced motions of a semi-submersible platform with four square columns, Part II: Effects of surface waves, external damping and draft condition. *Ocean Engineering*, 62, pp.10-24.

Hasebe, H., Watanabe, K., Watanabe, Y. and Nomura, T., 2009. Experimental study on the flow field between two square cylinders in tandem arrangement. *The Seventh Asia-Pacific Conference on Wind Engineering*, Taipei, 8-12 November 2009.

Knisely, C.W., 1990. Strouhal numbers of rectangular cylinders at incidence: a review and new data. *Journal of Fluids and Structures*, 4(4), pp.371-393.

Kumar, S.R., Sharma, A. and Agrawal, A., 2008. Simulation of flow around a row of square cylinders. *Journal of Fluid Mechanics*, 606, pp.369-397.

Lam, K. and Fang, X., 1995. The effect of interference of four equispaced cylinders in cross flow on pressure and force coefficients. *Journal of Fluids and Structures*, 9(2), pp.195-214.

Lam, K., Li, J.Y., Chan, K.T. and So, R.M.C., 2003a. Flow pattern and velocity field distribution of cross-flow around four cylinders in a square configuration at a low Reynolds number. *Journal of Fluids and Structures*, 17(5), pp.665-679.

Lam, K., Li, J.Y. and So, R.M.C., 2003b. Force coefficients and Strouhal numbers of four cylinders in cross flow. *Journal of Fluids and Structures*, 18(3), pp.305-324.

Lam, K. and Lo, S.C., 1992. A visualization study of cross-flow around four cylinders in a square configuration. *Journal of Fluids and Structures*, 6(1), pp.109-131.

Lesage, F. and Gartshore, I.S., 1987. A method of reducing drag and fluctuating side force on bluff bodies. *Journal of Wind Engineering and Industrial Aerodynamics*, 25(2), pp.229-245.

Li, J., Sun, J. and Roux, B., 1992. Numerical study of an oscillating cylinder in uniform flow and in the wake of an upstream cylinder. *Journal of Fluid Mechanics*, 237, pp.457-478.

Liu, C.H. and Chen, J.M., 2002. Observations of hysteresis in flow around two square cylinders in a tandem arrangement. *Journal of Wind Engineering and Industrial Aerodynamics*, 90(9), pp.1019-1050.

Luo, S.C., Chew, Y.T. and Ng, Y.T., 2003. Characteristics of square cylinder wake transition flows. *Physics of Fluids*, 15(9), pp.2549-2559.

Lyn, D.A., Einav, S., Rodi, W. and Park, J.H., 1995. A laser-doppler velocimetry study of ensemble-averaged characteristics of the turbulent near wake of a square cylinder. *Journal of Fluid Mechanics*, 304, pp.285-319.

Nakaguchi, H., Hashimoto, K. and Muto, S., 1968. An experimental study on aerodynamic drag of rectangular cylinders. *Journal of the Japan Society for Aeronautical and Space Sciences*, 16, pp.1-5.

Noda, H. and Nakayama, A., 2003. Free-stream turbulence effects on the instantaneous pressure and forces on cylinders of rectangular cross section. *Experiments in Fluids*, 34(3), pp.332-344.

Norberg, C., 1993. Flow around rectangular cylinders: pressure forces and wake frequencies. *Journal of Wind Engineering and Industrial Aerodynamics*, 49(1), pp.187-196.

Ootsuki, S., Fujii, K., Washizu, H. and Ohya, S., 1980. On the characteristics of three-component aerodynamic force and pressure distribution of a fixed two-dimensional recrtangular cylinder in a uniform flow. *Proceedings of the 6th Symposium on Wing Engineering, Japan Association for Wind Engineering*, Tokyo, pp153-159 (in Japanese).

Ota, T., Okamoto, Y. and Yoshikawa, H., 1994. A correction formula for wall effects on unsteady forces of two-dimensional bluff bodies. *Journal of Fluids Engineering*, 116(3), pp.414-418.

Saha, A.K., Muralidhar, K. and Biswas, G., 2000. Experimental study of flow past a square cylinder at high Reynolds numbers. *Experiments in Fluids*, 29(6), pp.553-563.

Sakamoto, H., Hainu, H. and Obata, Y., 1987. Fluctuating forces acting on two square prisms in a tandem arrangement. *Journal of Wind Engineering and Industrial Aerodynamics*, 26(1), pp.85-103.

Savkar, S.D., 1981. Buffeting force on rigid circular cylinders in cross flows. *Journal of Fluid Mechanics*, 105, pp.397-425.

Schewe, G., 1983. On the force fluctuations acting on a circular cylinder in crossflow from subcritical up to transcritical Reynolds numbers. *Journal of Fluid Mechanics*, 133, pp.265-285.

So, R.M.C., Liu, Y., Chan, S.T. and Lam, K., 2001. Numerical studies of a freely vibrating cylinder in a cross-flow. *Journal of Fluids and Structures*, 15(6), pp.845-866.

Stansby, P.K., 1974. The effects of end plates on the base pressure coefficient of a circular cylinder. *Aeronautical Journal*, 78, pp.36.

Tamura, T. and Miyagi, T., 1999. The effect of turbulence on aerodynamic forces on a square cylinder with various corner shapes. *Journal of Wind Engineering and Industrial Aerodynamics*, 83(1), pp.135-145.

Tutar, M. and Holdø, A.E., 2001. Computational modelling of flow around a circular cylinder in sub-critical flow regime with various turbulence models. *International Journal for Numerical Methods in Fluids*, 35(7), pp.763-784.

Waals, O.J., Phadke, A.C. and Bultema, S., 2007. Flow induced motions on multi column floaters. *ASME 2007 26th International Conference on Offshore Mechanics and Arctic Engineering*, American Society of Mechanical Engineers, San Diego, 10-15 June 2007, pp.669-678.

West, G.S. and Apelt, C.J., 1982. The effects of tunnel blockage and aspect ratio on the mean flow past a circular cylinder with Reynolds numbers between 10^4 and 10^5. *Journal of Fluid Mechanics*, 114, pp.361-377.

West, G.S. and Apelt, C.J., 1997. Fluctuating lift and drag forces on finite lengths of a circular cylinder in the subcritical Reynolds number range. *Journal of Fluids and Structures*, 11(2), pp.135-158.

Yen, S.C. and Liu, J.H., 2011. Wake flow behind two side-by-side square cylinders. *International Journal of Heat and Fluid Flow*, 32(1), 41-51.